Spectroscopy

Data Analysis Techniques in Astronomy and Planetary Science

BSc(Hons) Astronomy, Space Science and Astrophysics

Author: Lukasz R Tomaszewski (lrgt2)

Date: 4^{th} - 18^{th} March 2020

PH512 Assignment 4

Word Count: 1531

Contents

1 Spectroscopy Analysis

In astronomical image processing, spectroscopy is used to compute physical conditions of celestial bodies by separating their emitted light into wavelengths. Spectroscopy requires an additional optical instrument called a spectrograph, as all light passes through the telescope at the same point, the spectrograph separates all of the wavelengths before hitting the detector.

The spectrograph disperses all the light elements, two elements are: A glass prism refracts and separates the wavelengths at different angles, though the dispersion is unreliable as blue wavelengths disperse three times as much as the red wavelengths thus has a non-linear refraction angle. Diffraction grating is carefully shaping and spacing grooves into glass/ metal that diffract the light into different wavelengths, this is linear to the diffraction angle and the wavelength (Burnell and Berry 2000a).

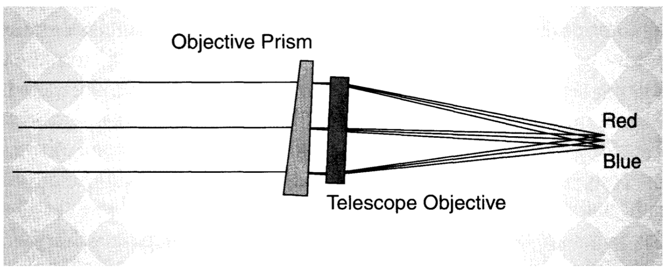

Figure 1a: Illustration of the objective prism spectrograph operating in front of a telescope. Source (Burnell and Berry 2000a).

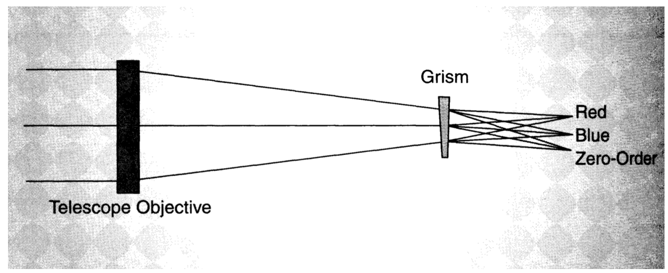

Figure 1b: Illustration of the grating-prism (grism) spectrograph operating behind the telescope. Source (Burnell and Berry 2000a).

There are 4 types of spectrographs: The objective prism in fig. 1a sits in front of the telescope so the refractive index of glass separates all the light into wavelengths as they exit the prism, this is mostly used as its used to survey stars faster. The grating-prism (grism) in fig. 1b sits behind the telescope lense and refracts the light into wavelengths, this operation is cheaper as it operates 'diffraction grating'. The slit is place in front of the telescope and isolates the celestial body, thus narrows the light emitted for a prism/ grism to operate, the last is fiber-fed that allows the light to travel through optical glass fibers to the prism/grism separate from the telescope (Burnell and Berry 2000a).

2 Dispersion & Resolving Power

Some properties of the spectrum/ spectra are dispersion and resolving power (spectral resolution). Dispersion is the light that diffracts off a prism/ grism and disperses into wavelengths, its simply the rate of change of the wavelength in relation to the spectrum distance, it can be computed into nanometers per pixel:

$$\text{Dispersion} = \text{D} = \frac{\text{Free Spectral Range}}{\text{Number of Pixels}} \quad [\text{nm/pixel}] \tag{1}$$

Where the 'Free Spectral Range' is the wavelength range in the relevant spectrum: short-wavelengths of 360nm, ultraviolet wavelengths of 1100nm, infrared wavelengths of 740nm but and for stellar spectral objects at 150nm. The resolving power is a mixture of factors that separate lines which have a small difference in wavelength, such factors include: width of the slit, size of the star image, the fiber tip and the dispersion of the prism, grating and quality of the optics used (Burnell and Berry 2000a). Its computed by:

$$\text{Resolving Power} = \text{R} = \frac{\text{Wavelength}}{\text{Resolution}} \quad [\text{Dimensionless}] \tag{2}$$

The resolving power is most commonly twice that of the dispersion, its used to classify star types between 150 and 100 resolving power, whereas professional astronomers used a resolving powers up to 100,000 (Burnell and Berry 2000a).

3 Spectroscopy Method

Using the 'spectroscopy tool' in the AIP4WIN software on the image file 'VegaSpectrum.fts' of a zero magnitude type A0V star Vega which was captured using a 6-inch objective prism, the image is already calibrated through dark frame subtraction and flat-fielding (Burnell and Berry 2000b).

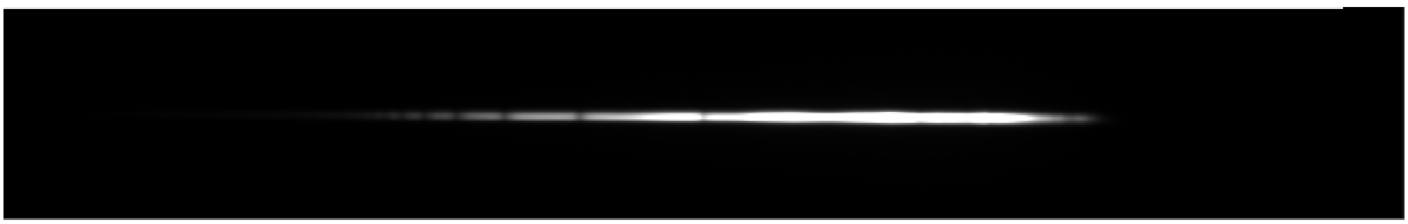

Figure 2a: Infrared image of the Vega ready to undergo spectroscopy,
loaded into AIP4WIN software under 'VegaSpectrum.fts'.

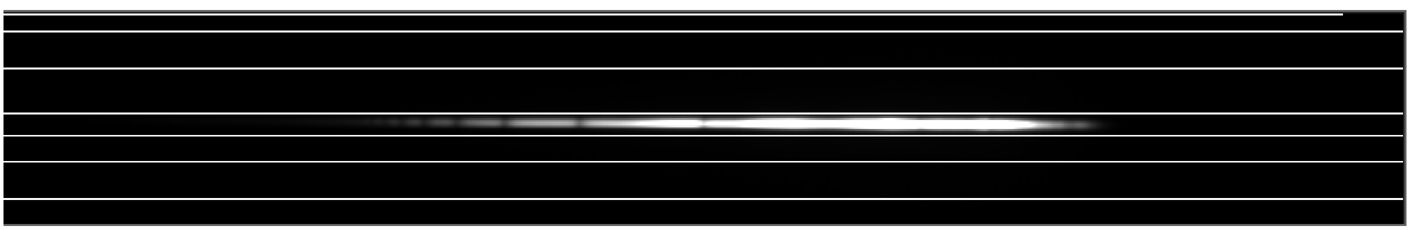

Figure 2b: Infrared image of Vega with the spectroscopic above sky, spectrum
and the bottom sky boundaries marked on 'VegaSpectrum.fts'.

By invoking the spectroscopy tool in fig. 3a, six boundary positions are plotted: two around the actual spectral region and the other four (two above and two below the spectral object) measuring the sky background. The 'objective mode' is selected as it takes a median of sky background across the entire image and this median is subtracted against the spectral object to further isolate the emitted light only from the spectral object. To set the 'vertical scale type' as linear to produce a set valued graph as seen in fig. 3a, pressing 'Save' gives a tabular of data which is used to produce the graph in fig. 3a and reproduce to provide more detail as seen in fig. 3b. As the image (fig. 3b) shows a horizontal profile of light of the Vega star (fig. 2a), it shows the intensity of light in relation to the the position of the star. It plots the light intensity as the pixel value from one side to the other while measuring the counts of intensity. The pixel value can be changed into wavelength using a calibration graph that measuring wavelength value instead of pixel value but by comparing the peaks of data, its possible to match the pixel value to wavelength value and therefore find the type of light it emits from the electromagnetic light spectrum.

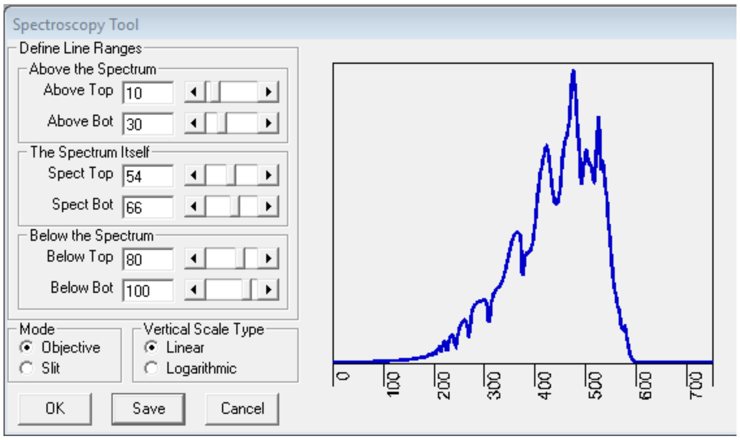

Figure 3a: AIP4IWIN 'spectroscopy tool' above sky, spectrum and the bottom sky boundary settings for fig. 2b and its spectroscopic graph.

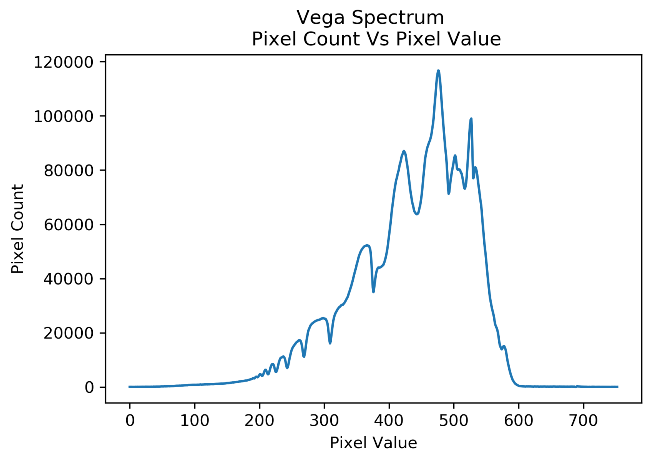

Figure 3b: Python reconstruction of the Vega spectrum graph in fig. 3a, showing the individual pixel counts for each spectroscopic pixel value.

4 Asteroid Spectroscopy

4.1 Asteroid Spectroscopy

By obtaining the image files 'AST_rot_tr.fits', 'HeAr_rot_tr.fits' and 'SA_rot_tr.fits' and utilizing the spectroscopy method outlined in section 3, the spectroscopic boundaries were set for each image as seen in the figure 4a,b,c and as tabulated in table 1. Which the spectroscopic data was retrieved and it was plotted in figure 5a,b,c. As the 'HeAr_rot_tr.fits' image (fig. 4b) has no sky background subtraction as the captured spectrum is vertical in nature and thus will provide a fluctuating light profile. The 'SA_rot_tr.fits' image (fig. 4c) is the same image to that of the 'AST_rot_tr.fits' image (fig. 4a) but it is captured by placing a slit in front of the telescope and blocks out all the sky background.

AIP4IWIN 'spectroscopy tool' above sky, spectrum and bottom sky boundary settings						
Spectrum	'AST_rot_tr.fits'		'HeAr_rot_tr.fits'		'SA_rot_tr.fits'	
Setting	Top	Bottom	Top	Bottom	Top	Bottom
Above	100	120	223	243	330	350
Spectrum	0	0	200	220	0	0
Below	90	110	223	243	330	350

Table 1: AIP4IWIN 'spectroscopy tool' above sky, spectrum and the bottom sky boundary settings for fig. 4a, fig. 4b and fig. 4c.

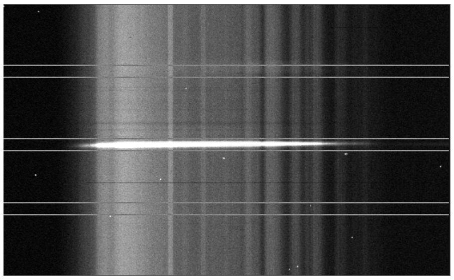

Figure 4a: ’AST_rot_tr.fits’ image with it’s spectroscopic boundaries valued in table 1

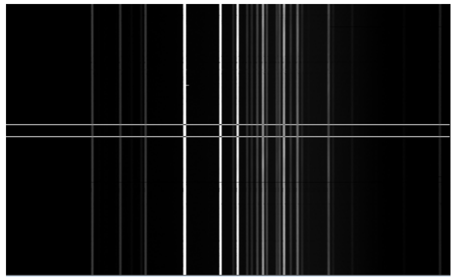

Figure 4b: ’HeAr_rot_tr.fits’ image with it’s spectroscopic boundaries valued in table 1

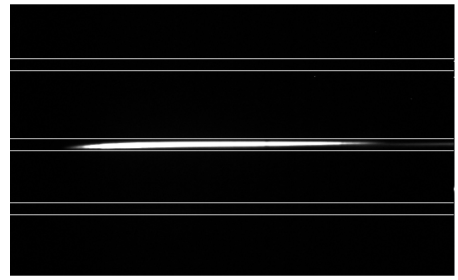

Figure 4c: ’SA_rot_tr.fits’ image with it’s spectroscopic boundaries valued in table 1

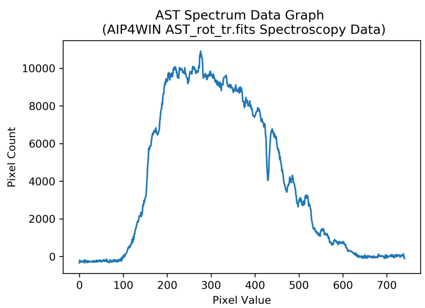

Figure 5a: Graphical ’AST_rot_tr.fits’ spectroscopy data.

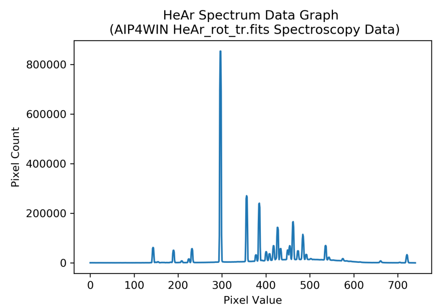

Figure 5b: Graphical ’HeAr_rot_tr.fits’ spectroscopy data.

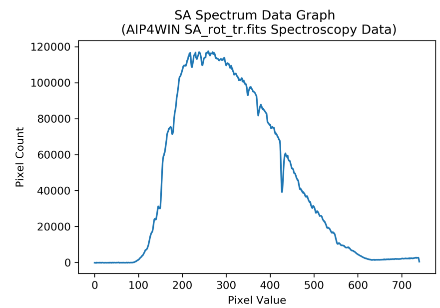

Figure 5c: Graphical ’SA_rot_tr.fits’ spectroscopy data.

4.2 Asteroid Calibration

A calibration is in order to relate the pixel values with wavelength, this is achieved by physically comparing a set data graph seen in fig. 6b with the experimental data graph resourced in section 4.1. The calibration is tabulated in table 2, where the wavelength in angstrom (Å) is converted to nanometres (nm) by the definition of 10Å = 1nm (Burnell and Berry 2000a).

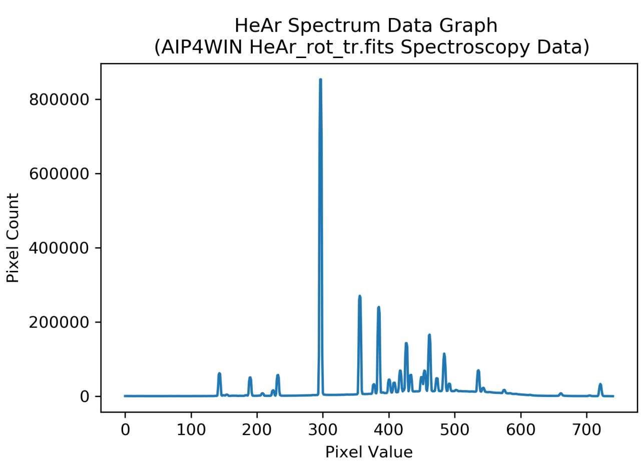

Figure 6a: Graphical ’HeAr_rot_tr.fits’ spectroscopy data.

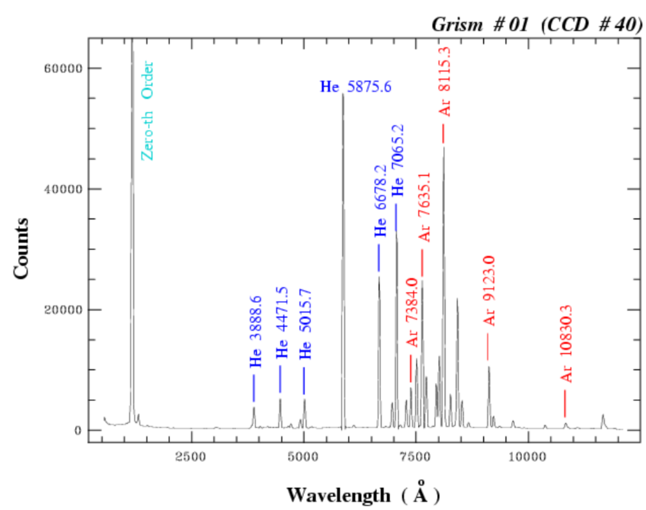

Figure 6b: Calibration image for ’HeAr_rot_tr.fits’ image.

Calibration data of experimental and theory data									
Helium					Argon				
Element	λ (Å)	λ (nm)	Pixel Values	Spectrum	Element	λ (Å)	λ (nm)	Pixel Values	Spectrum
He 3888.6	3888.6	388.9	140	UV	Ar 7384.0	7384.0	738.4	410	IR
He 4471.5	4471.5	447.2	190	Blue	Ar 7635.1	7635.1	763.5	425	IR
He 5015.7	5015.7	501.2	230	Green	Ar 8115.3	8115.3	811.5	485	IR
He 5875.6	5875.6	587.6	295	Yellow	Ar 9123.0	9123.0	912.3	530	IR
He 6678.2	6678.2	667.8	355	Red	Ar 10830.3	10830.3	1083.0	660	IR
He 7065.2	7065.2	706.5	385	IR					

Table 2: Calibration data of fig. 6a and fig. 6b, by comparing peaks to fix a wavelength to a pixel value.

By associating the pixel value with a given wavelength, its now possible to specify on the experimental data graphs that at a certain pixel values equals to a certain wavelength. For example using table 2 at a pixel value of 410, its wavelength value is 738.4nm. This now allows for comparison with the electromagnetic light spectrum to specify which type of light is at each individual pixel value by using fig. 7a. Thus as seen in table 2 the spectrum type is shown as each element is categorised in each spectrum and each colour of the visible spectrum

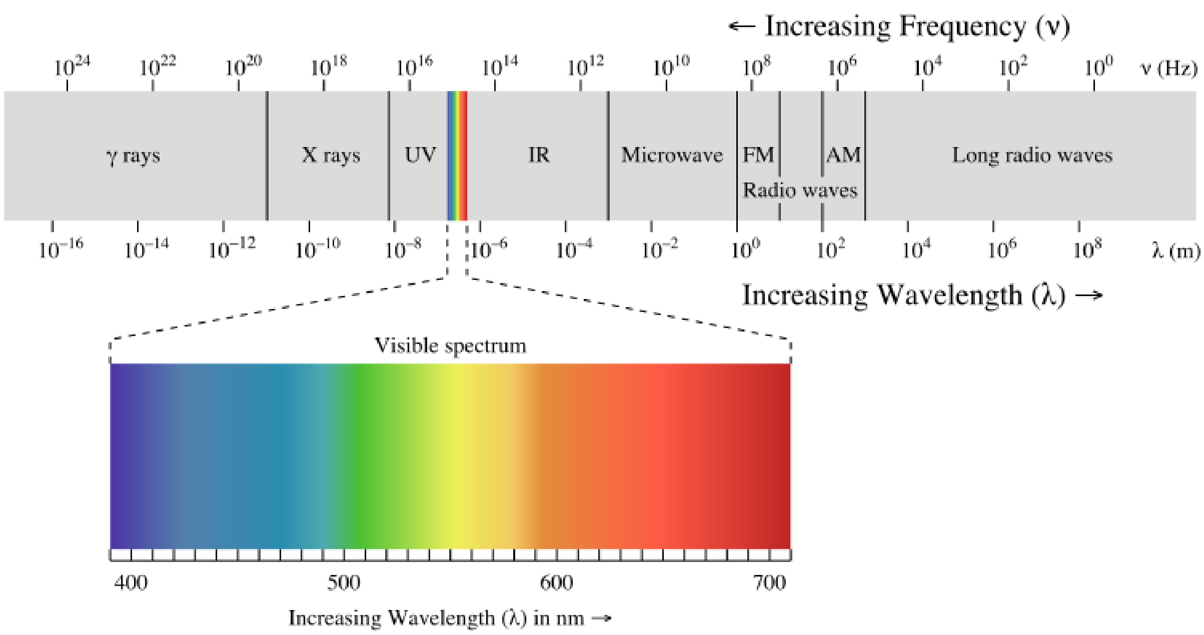

Figure 7a: Illustration of the electromagnetic spectrum (*The electromagnetic spectrum* 2020).

By using the calibration of wavelength and or determining the wavelength per pixel in eq. (4), its seen that the 'Hear_rot_tr.fits' image (fig. 5b) emits in the yellow spectrum at its peak, whereas the 'AST_rot_tr.fits' image (fig. 5a) and the 'SA_rot_tr.fits' emits in the green spectrum. On a side note its possible to calculate the dispersion as the factors of eq. (1) are known:

$$\text{Dispersion} = \text{D} = \frac{\text{Free Spectral Range}}{\text{Number of Pixels}} = \frac{150\times10^{-9}\text{m}}{740\text{ Pixels}} = 0.203\text{ nm/pixel} \tag{3}$$

Its possible to calculate the resolving power as well for each individual wavelength using eq. (2) and taking the resolution of the telescope.

4.3 Solar Analog Analysis

By sourcing the data from fig. 4a and fig. 4c where instead of taking the objective and background sky light together and letting the software subtract it itself, they are taken separately where the background sky is subtracted against the objective is done manually. Using fig. 6b its possible to find the best fitting polynomial which is specified as:

$$\lambda_i = a + bx_i \tag{4}$$

$$a = \lambda_i - (bx_i) \rightarrow 3888.6 - (13.53 * 143) = 1953.81 \tag{5}$$

$$b = \frac{\lambda_2 - \lambda_1}{x_2 - x_1} \rightarrow \frac{9123.0 - 3888.6}{530 - 143} = 13.53 \tag{6}$$

Using eq. (4), its possible to work out the wavelength per pixel (λ_i) and x_i is pixel value where a and b are constants, this allows further analysis of the image in relation to the electromagnetic spectrum. To normalise the data shown in fig. 8a and fig. 8b, where the values of the highest peak of the graph was taken and the individual spectrum value on the data set was divided by this value at the highest peak, this will normalise the graph so the axis are all the same so the asteroid and the solar analog images can be accurately compared, the y-axis for both image were of different values where now they are the same.

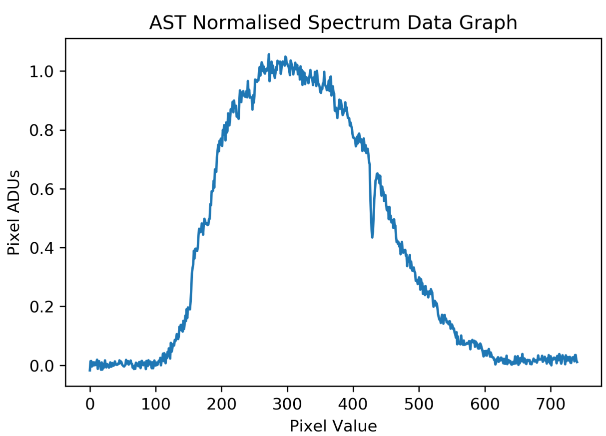

Figure 8a: Graphical 'AST_rot_tr.fits' normalised spectroscopy data.

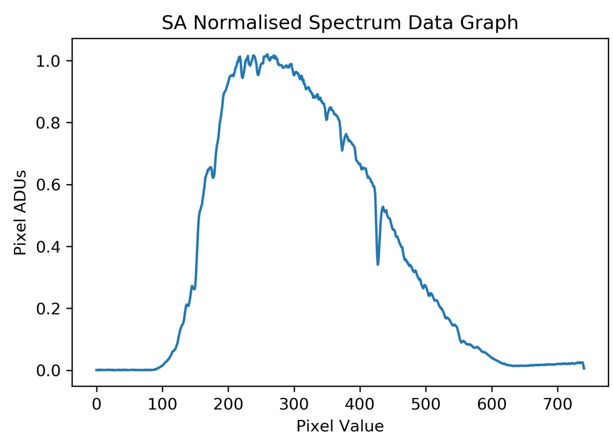

Figure 8b: Graphical 'SA_rot_tr.fits' normalised spectroscopy data.

The normalised data is plotted in fig. 8a and fig. 8b where the normalised will equal the axes where they can be plotted against each other in fig. 9, as they have been normalised, comparing them becomes easier as it can be seen that the moving the slit of the telescope for the 'SA_rot_tr.fits' doesn't allow for background sky subtraction thus altering the data set between both the asteroid image and the solar analog image. By diving the solar analog data with the asteroid data, the difference in results is shown more in fig. 10, this shows the difference in results between the using a slit and subtracting background sky counts.

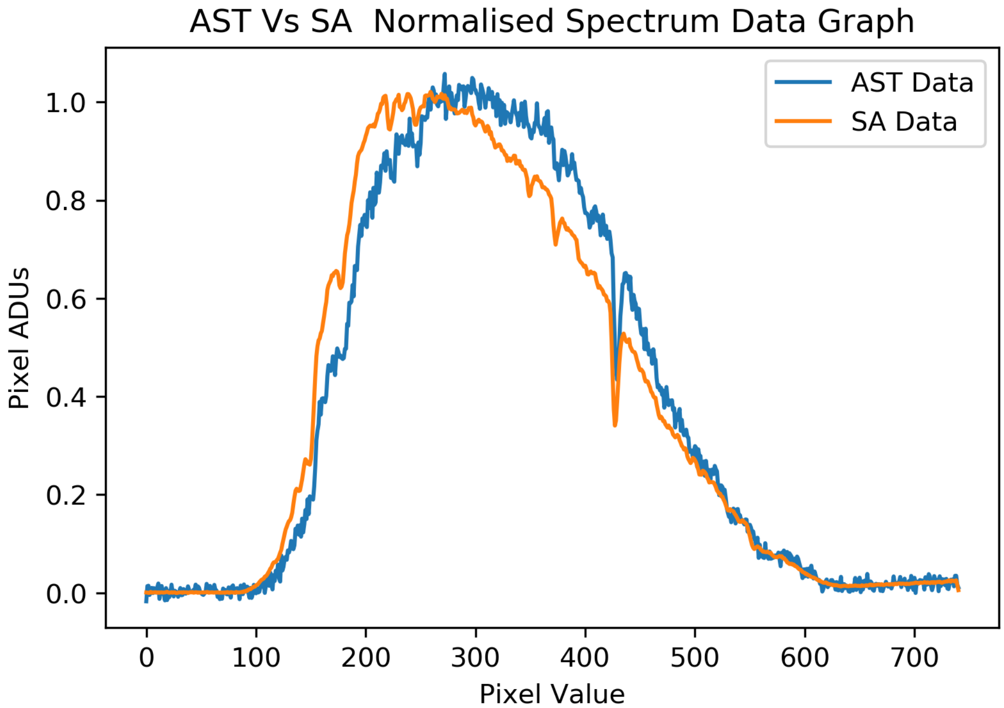

Figure 9: Graphical 'AST_rot_tr.fits' against 'SA_rot_tr.fits' normalised spectroscopy data.

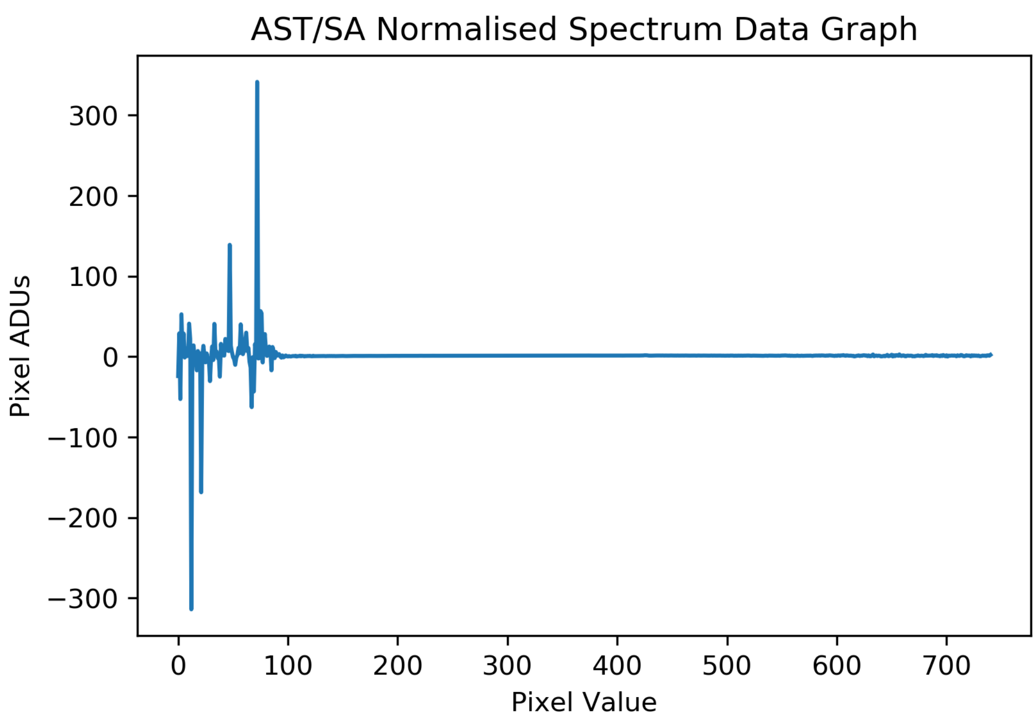

Figure 10: Graphical representation of the 'AST_rot_tr.fits' data divided by the 'SA_rot_tr.fits' data.

5 Asteroid Discussion

By using (Mansour et al. 2020) they used spectroscopy to determine the distribution of basaltic asteroids, they analysed and striped the data off each asteroid reported in the MOVIS-C catalogue from the Minor Planet center, all the data was normalised and three main types of meteorite's were compared with each other. They further went on to classify the distribution in terms of wavelength where they further used the data to determine the absolute magnitude of each basaltic asteroid.

The results in this report were normalised like in (Mansour et al. 2020), as to allow accurate comparison of multiple asteroids and provide further analysis of the difference between each asteroid in this experiment and or in (Mansour et al. 2020). This shows that not only can spectroscopy be used to determine the colour of the electromagnetic spectrum of the light emitted off the objective spectrum but through further analysis can help in astrometry and photometry. This proves that all of spectroscopy is another tool in the belt of image processing that continues to assist astronomers in observering the universe.

References

Burnell, J. and R. Berry (2000a). *The Handbook of Astronomical Image Processing*. 2th. Richmond, Virginia: Willmann-Bell, 2005, ISBN: 9780943396828, Pages: 303-320.

— (2000b). *The Handbook of Astronomical Image Processing*. 2th. Richmond, Virginia: Willmann-Bell, 2005, ISBN: 9780943396828, Pages: 642-644.

Mansour, J. A. et al. (Feb. 2020). "Distribution and spectrophotometric classification of basaltic asteroids". In: 491, pp. 5966–5979.

The electromagnetic spectrum (2020). URL: `https://www.khanacademy.org/science/physics/light-waves/introduction-to-light-waves/a/light-and-the-electromagnetic-spectrum`.